Comparing Evaporative Sources of Terrestrial Precipitation and Their Extremes in MERRA Using Relative Entropy

Paul A. Dirmeyer[1,2], Jiangfeng Wei[3], Michael G. Bosilovich[4], and David M. Mocko[4,5]

[1] Department of Atmospheric, Oceanic and Earth Sciences, George Mason University, Fairfax, Virginia, USA

[2] Center for Ocean-Land-Atmosphere Studies, Institute of Global Environment and Society, Calverton, Maryland, USA

[3] Jackson School of Geosciences, University of Texas at Austin, Austin, Texas, USA

[4] Global Modeling and Assimilation Office, NASA Goddard Space Flight Center, Greenbelt, Maryland, USA

[5] SAIC, Greenbelt, Maryland, USA

1 **Abstract:**

2 A quasi-isentropic back trajectory scheme is applied to output from the Modern Era

3 Retrospective-analysis for Research and Applications and a land-only replay with

4 corrected precipitation to estimate surface evaporative sources of moisture

5 supplying precipitation over every ice-free land location for the period 1979-2005.

6 The evaporative source patterns for any location and time period are effectively

7 two-dimensional probability distributions. As such, the evaporative sources for

8 extreme situations like droughts or wet intervals can be compared to the

9 corresponding climatological distributions using the method of relative entropy.

10 Significant differences are found to be common and widespread for droughts, but

11 not wet periods, when monthly data are examined. At pentad temporal resolution,

12 which is more able to isolate floods and situations of atmospheric rivers, values of

13 relative entropy over North America are typically 50-400% larger than at monthly

14 time scales. Significant differences suggest that moisture advection may be key to

15 precipitation extremes. Where evaporative sources do not change significantly, it

16 implies other local causes may drive the extremes.

17

18

1. Introduction

Rain or snow falling over any particular location is composed of condensed water vapor that entered the atmosphere as surface evaporation from a range of upstream locations. Surface and atmospheric conditions along the paths of moisture advection determine the ultimate sources of evaporative moisture, which generally have a combination of oceanic and terrestrial origins. Knowledge of the sources of moisture supplying precipitation over a particular location could be used to understand how upstream surface changes may affect local hydrology, and potentially to aid prediction (e.g., Dirmeyer and Kinter 2010; Bagley et al. 2012, Spracklen et al. 2012).

There are three basic approaches to estimating the connection between surface evaporation from specific locations and subsequent precipitation of that water. The simplest but most limited in capabilities is the bulk method, which relies on regional atmospheric moisture budgets at relatively long time scales, typically one month (Brubaker et al. 1993). This approach is most often used to estimate precipitation recycling as derived by Budyko (1974) – the portion of precipitation over a given area that originated as evaporation within the same area (e.g., Eltahir and Bras 1994, Gong and Eltahir 1996, Trenberth 1999). Burde et al. (1996) showed that this method has an implicit assumption of one-dimensionality that causes errors, which can be accounted for in a two-dimensional derivation, further refined by Burde and Zangvil (2001). These approaches typically use global atmospheric reanalyses as the source of the necessary meteorological fields. Dominguez et al. (2006) recognized the lack of water budget closure in reanalyses could affect the bulk

42 estimates, but decided the impact was small over the United States. Bisselink and

43 Dolman (2008) came to the same conclusion for Europe. This approach has been

44 extended to differentiate solely between terrestrial and oceanic moisture sources

45 (e.g., Gimeno et al. 2010; Goessling and Reick 2011). van der Ent (2010) developed a

46 backtracking model based on the vertically-integrated moisture transport and the

47 constraints of atmospheric water balance, but still in the Eulerian framework. Keys

48 et al. (2012) developed an interesting variant on that approach to estimate the

49 "precipitation-sheds" of regions, to assess their potential vulnerability to changing

50 evapotranspiration with land use changes.

51 Another approach is to include water vapor tracers directly within a three-

52 dimensional model of the atmosphere. This approach typically accomplishes the

53 tracing in a Lagrangian framework, providing a highly accurate set of trajectories for

54 water vapor parcels. Druyan and Koster (1989) tagged water vapor evaporation

55 from specific regions in a global model to compare moisture sources during wet and

56 dry conditions over the Sahel. Bosilovich and Sun (1999) performed a similar

57 analysis with a regional model over the central United States. Numaguti (1999)

58 performed a continental-scale tracer analysis over Eurasia, while Bosilovich and

59 Schubert (2002) performed a global study of evaporative sources of precipitation

60 using tracers in a global atmospheric model. Stohl and James (2004) used a

61 dispersion model driven by reanalyses to examine a case study of moisture

62 transport over Europe, and a one-year global assessment. Stohl and James (2005)

63 applied the method to diagnose oceanic moisture sources to major river basins.

64   A variation on the tracer approach is to use water isotopes as the markers

65   (Henderson-Sellers et al. 2004).   Terrestrial versus oceanic sources can be

66   distinguished in this manner. Kurita et al. (2004) were able to trace the changing

67   sources of precipitable water across Russia from isotope measurements. Salati et al.

68   (1979) did this for the Amazon basin, and Tian et al. (2001) measured the

69   northward penetration of the South Asian monsoon circulation over Tibet using

70   isotopic measurements, among many other regional studies.   An atmospheric

71   isotope model was employed by Yoshimura et al. (2004) in a study of moisture

72   sources for the Asian monsoon.

73   The bulk approaches mentioned above suffer several shortcomings, including errors

74   introduced by the coarse temporal and vertical resolution of the methodology and

75   data, lack of water budget closure in reanalysis data sets, and neglect of nonlinear

76   processes and asymmetrical moisture advection.   Tracers embedded within

77   atmospheric models can have "perfect" tracking of water vapor at the full spatial

78   and temporal resolution.   However, they tend to add great expense to the

79   simulations, especially in terms of computer memory use and data storage, as each

80   additional evaporative source requires another full three-dimensional state variable

81   to be carried in the model and integrated forward in time. Also, calculations from

82   these methods are subject to all the systematic errors of the model, which can often

83   be substantial for quantities like precipitation and evaporation (Kanamitsu et al.

84   2002). Models can be constrained by data assimilation, but the assimilation of

85   humidity violates conservation and closure of the water budget, which cannot be

86   handled elegantly by tracers.

87   A compromise is to calculate the tracers a posteriori from atmospheric analyses at a

88   high spatial and temporal resolution that resolves the synoptic-scale fluctuations in

89   water vapor, and even the diurnal cycle, as well as the vertical structure of moisture

90   in the atmosphere, but may not use data from every time step of the atmospheric

91   model producing the analysis.   When using reanalyses as the source of the

92   meteorological forcing data, the issue of lack of closure of the water budget still

93   arises, but is less severe, particularly when observed precipitation data are used to

94   constrain the model simulations.   This method has been used to independently

95   validate other methods of estimating precipitation recycling and its variability

96   (Brubaker et al. 2001; Sudradjat et al. 2003; Dirmeyer and Brubaker 2007), define

97   regional links between tropical moisture and mid-latitude floods (Dirmeyer et al.

98   1999; Reale et al. 2001; Sudradjat 2002; Turato et al. 2004; Dirmeyer and Kinter

99   2009, 2010, Wei et al. 2012), quantify links between nations through the

100   atmospheric branch of the hydrologic cycle (Dirmeyer et al. 2009), estimate remote

101   impacts of tropical land use change (Bagley et al. 2012) and study the fate of

102   evaporated irrigation water (Tuinenburg et al. 2012; Wei et al. 2013).

103   In this paper, we present results of this type of approach, the quasi-isentropic back-

104   trajectory scheme of Dirmeyer and Brubaker (2007) applied globally at a higher

105   spatial resolution than it has been previously, using NASA reanalysis products.   In

106   addition to determining sources of evaporated moisture supplying precipitation and

107   estimating recycling ratios, differences in the distribution of sources during

108   droughts and wet intervals are quantified.

109   Section 2 describes the data sets used, the back-trajectory technique that estimates

110   the distribution of evaporative sources for moisture supplying precipitation over

111   any location, and a robust statistical method to compare distributions of evaporative

112   sources. The basic distributions of moisture sources are presented in Section 3.

113   Section 4 investigates how source regions vary in the cases of precipitation

114   extremes. Discussion is presented in Section 5.

115

116   **2. Data and Methods**

117   The global meteorological analysis used for this study is the Modern Era

118   Retrospective-analysis for Research and Applications (MERRA; Rienecker et al.

119   2011). MERRA uses the Goddard Earth Observing System (GEOS-5) atmospheric

120   model and data assimilation system at a resolution of 2/3° longitude by 1/2°

121   latitude, overlying the Catchment land model (Koster et al. 2000; Ducharne et al.

122   2000). MERRA placed an emphasis on improved simulation of the global hydrologic

123   cycle, assimilating instantaneous precipitation rates (Decker et al. 2011).

124   Nevertheless, model biases and discontinuities from changing satellite platforms

125   introduce precipitation errors (Robertson et al. 2011), which affect the surface

126   water budget.

127   Reichle et al. (2011) used the replay feature of GEOS-5 to generate a land-only

128   analysis called "MERRA-Land", where precipitation from the observationally based

129   Global Precipitation Climatology Project (GPCP; Huffman et al. 2009, Xie et al. 2003)

130   is used to correct MERRA precipitation. This results in estimates of evaporation and

131 other surface quantities that are more consistent with observations.   Dirmeyer

132 (2011) showed that MERRA-Land surface flux data produce estimates of land-

133 atmosphere coupling that are much more consistent with a wide range of other data

134 sets than MERRA.

135 These data are used to drive the quasi-isentropic back trajectory scheme that

136 estimates the distribution of surface evaporation that supplies precipitation as a

137 function of space and time (Brubaker et al. 2001; Dirmeyer and Brubaker 2007). It

138 is a Lagrangian method that traces the advection of moisture back in time from

139 precipitation events, and uses upstream evaporation and precipitable water

140 estimates to determine the probabilistic distribution of surface evaporation

141 supplying the precipitated water vapor to the atmosphere. Data are aggregated in

142 time over 5-day and monthly intervals, with a spatial distribution for every land

143 surface grid point.   On a high-resolution global grid such as MERRA, this generates a

144 very large set of two dimensional source fields. The source fields for a set of grid

145 boxes, delineating a river basin, nation, or any arbitrary land area, can be easily

146 calculated by aggregation from the resolution grid.

147 The spatial pattern of surface evaporative sources is effectively a two-dimensional

148 probability distribution. There exist objective quantitative methods to determine

149 the degree of similarity between two probability distributions. Relative entropy,

150 which also goes by other names such as information divergence and Kullback

151 Leibler divergence, is such a quantification (cf. DelSole and Tippett 2007). The

152 relative entropy between two distributions p and q on a discrete spatial grid is

153 defined as (Kleeman 2002):

$$RE_{p,q} = \sum_i p(i) \log \frac{p(i)}{q(i)}$$

where i is the index of the grid points (in our case it is two dimensional but it applies over any number of dimensions) and each of the distributions are defined as having a sum total of unity. Thus, we must normalize any spatial distributions before applying this method. For two identical distributions, RE=0. Any deviations will increase the value of RE. $RE_{p,q} \neq RE_{q,p}$, but the ranking is preserved with either choice of p and q, and RE is invariant to linear and nonlinear transforms.

What is not straightforward, however, is quantification of a statistical significance in the difference between two distributions when they do not share identical or well-described low-order moments (DelSole and Tippett 2007). For example, the significance in the shift between two normal distributions can be quantified, but if one or both distributions are non-normal, or otherwise do not share basic shape parameters, significance can only be determined by Monte-Carlo bootstrap techniques. We have used such an approach, which is described in the next section along with some characteristics of the climatology of evaporative sources.

3. Evaporative Sources

Figure 1 shows the total evaporative source supplying precipitation over land (Antarctica and other ice-covered points excluded) aggregated from monthly data for each season. Two sets of estimates are used; one based on MERRA with precipitation corrected by GPCP and MERRA-Land estimates of evaporation (top panels), as well as one based solely on the original MERRA output. The bottom

8

176   panels show the difference between evaporative source estimates with MERRA

177   alone minus the estimates where MERRA-Land is used for terrestrial evaporation

178   and precipitation estimates. Looking first at the top panels, there is a clear

179   seasonality to both the terrestrial and oceanic sources of evaporation supplying

180   precipitation over land. The strongest sources tend to be in low latitudes over land

181   and adjacent open oceans, although a number of areas in the northern mid-latitudes

182   become prominent in JJA. The strength of oceanic sources correlate strongly to the

183   distance to shore, but there are exceptions (e.g., the closed 30 kg m^{-2} contour in the

184   North Pacific during JJA).

185   The bottom panels of Fig 1 show that MERRA evaporation (and precipitation) over

186   land is generally much higher than GPCP observations suggest should be the case.

187   Yet, MERRA has a very strong cross-equatorial gradient in terrestrial precipitation,

188   with erroneously dry conditions over much of South America and Africa. These

189   systematic errors greatly impact the estimates of evaporative sources – motivating

190   our use of MERRA-Land for our calculations. The fraction of evaporated moisture

191   feeding precipitation over the land areas in the top panels is 52%, 62%, 50% and

192   45% during MAM, JJA, SON and DJF respectively. When the MERRA output with its

193   precipitation biases is used to estimate evaporative sources, the terrestrial

194   percentages increase to 55%, 64%, 52% and 46%.

195   Figure 2 gives a notion of how regional evaporative sources appear. The mean

196   surface evaporative sources supplying precipitation to four sections of the

197   conterminous United States are presented, normalized to indicate the percentage of

198   the total supplied from each MERRA grid box. This and all future figures are based

199   on the estimates using the corrected precipitation and MERRA-Land evaporation.

200   The source into the western U.S. is seen to have a long fetch stretching from the

201   subtropical North Pacific, indicative of the "atmospheric rivers" that supply much of

202   the moisture for winter rain and snow (e.g., Dettinger et al. 2011). There is also a

203   great deal of moisture supplied from terrestrial evapotranspiration over northern

204   California, Oregon and Washington, according to this analysis.

205   The Great Plains and eastern Rockies have an evaporative source that mainly comes

206   from the western Gulf of Mexico, as well as terrestrial areas in the southern part of

207   the region, and sporadic moister localities across the inter-mountain West.   The

208   region of the Pacific off the coast of Baja California is also a moisture source prior to

209   the onset of the North American monsoon (cf. Brubaker et al. 2001).

210   The bottom panel of Fig 2 shows the evaporative source supplying precipitation

211   over the states of the Mississippi Basin mainly east of the Great Plains. This area

212   also shows a major oceanic source from the Gulf of Mexico, but with more extent

213   into the northern Caribbean Sea (cf. Dirmeyer and Kinter 2010), and little moisture

214   coming from the west.   There is again a substantial terrestrial source over the

215   southern and central portions of the area.

216   The top panel also shows the evaporative source for the East Coast, which shows

217   much more of a source from the open Atlantic than does the Mississippi Basin area.

218   Again, little moisture supplying precipitation comes from the west – most comes

219   from the south.   Recycling over each area, defined as the fraction of the total

220   evaporative moisture source that lies within the boundaries of the region, are 12%,

221   22%, 19% and 14% for the West, Great Plains, Mississippi Valley and East Coast

222 respectively. For the same regions, oceanic moisture sources account for 81%, 48%,

223 46% and 53% of precipitation.

224 Figure 3 shows for each season the fraction of precipitation at each grid point that

225 originated from evaporation over land. The pattern of mean low-level flow is

226 evident in the patterns. In mid-latitudes, where winds are predominantly from the

227 west, the west coasts receive predominantly moisture of oceanic origin, and the

228 eastern sides of continents have much more moisture of terrestrial origin. The

229 pattern is reversed at low latitudes. The global mean fractions of terrestrial sources

230 of moisture supplying terrestrial precipitation are 46%, 50%, 40% and 38% during

231 boreal spring, summer, fall and winter respectively.

232 There are also some pronounced regional seasonal cycles. Large areas of central

233 Asia into Siberia receive more than 90% of their precipitation from land

234 evaporation during spring and summer. The region around Ethiopia and Sudan has

235 a large oscillation between oceanic sources in the winter and spring, and terrestrial

236 sources during summer into fall. Much of southern Africa has a similar variation,

237 but six months out of phase. The general east-west gradient over North America is

238 maintained through out the year, but fluctuates from a predominance of marine

239 sources in winter to a much larger portion of continental sources in summer. Most

240 of Eurasia also shows the same annual cycle as North America.

241 Very strong gradients are evident across the steep terrain of the Himalayas, with

242 large terrestrial proportions over the Tibetan Plateau, and predominant oceanic

243 sources to the south. This gradient extends northeastward across China. There are

244 also fairly strong gradients along the Rift Valley of Africa, but curiously there is little

245   apparent signature of the Rocky Mountains or Andes except in the immediate

246   vicinity of the Altiplano.

247   The distance from each terrestrial grid point to the central moment of the

248   climatological evaporative source is shown in Fig 4. This gives an indication of the

249   average distance water vapor travels in the air before falling as rain or snow at that

250   location. Arid regions far from open ocean typically have the largest values, with

251   substantial areas of the Sahara (all seasons) and south-central Asia (all except JJA)

252   showing values in excess of 4000km. The shortest fetches are found in subtropical

253   regions during the local rainy season. Parts of subtropical South America, southern

254   Africa and northwestern Australia show typical distances of less than 500km, as

255   does a band across the Sahel to Ethiopia, particularly during JJA. These areas show

256   some persistence of the relatively short transport distances even in the dry season.

257   Surprisingly, the distances are somewhat longer in the deep tropics. The effect of

258   the annual cycle of winds and terrestrial evaporation are evident over the middle

259   and high latitudes of the Northern Hemisphere. Distances are shorter in the

260   summer when land evapotranspiration is greatest and winds are lighter.

261   The remainder of the paper discusses the quantification of evaporative sources

262   associated with hydrologic extremes. To do so requires quantification of the

263   deviation of an evaporative source from its climatology. The method of relative

264   entropy was described in Section 2. Figure 5 shows the average value of the relative

265   entropy calculated between the climatological pattern of evaporative sources and

266   each of the 27 individual years, on a monthly basis then aggregated to seasonal,

267   calculated for every land grid point. Small values suggest there is very little

12

268   variation in the probability distribution, represented by the normalized evaporative

269   source like those depicted in Fig 2 for area totals. Small values predominate over

270   the tropics, monsoon regions during the wet season, and humid regions in general.

271   Large values are most likely over arid regions, suggesting a great deal of interannual

272   variability in moisture sources there.

273   However, there is not a one-to-one correspondence between precipitation and the

274   interannual variability in moisture sources. For example, northern Australia shows

275   very large RE values during MAM and a minimum during SON, even though DJF is

276   the wet season and JJA is the core of the dry season. Likewise, over the western

277   Great Plains there is a clear maximum in relative entropy, and thus peak year-to-

278   year variability in moisture sources, during SON, which is a period of transition from

279   a late spring peak to a winter minimum in total precipitation.

280

281   **4. Extremes**

282   The relative entropy statistic provides a handy measure of the difference between

283   any two patterns of evaporative sources. As an example of the application of the

284   relative entropy calculation, the differences between the global estimates of

285   evaporative sources of terrestrial precipitation shown in Fig 1 result in relative

286   entropies of 0.30, 0.76, 0.37 and 0.14 for MAM, JJA, SON and DJF respectively. This

287   quantifies what can be seen by eye, that the largest differences appear during JJA,

288   and the two estimates for DJF are rather similar on a global scale.

289   Here, we use relative entropy to determine the difference from the climatological

290   pattern of evaporative sources at each land grid point for specific climatic

291   categories, namely the months and years with the greatest or least precipitation.

292   With this approach, we may determine whether changes in the sources of moisture

293   supplying precipitation (i.e., changes in circulation, moisture advection, and remote

294   evaporation) are significant contributors to precipitation extremes. For locations

295   where the answer is negative, other causes may be at play, such as local conditions

296   like atmospheric stability, convective potential or land surface feedbacks, or

297   possibly other large-scale factors not discernable from our back-trajectory analysis.

298   Figure 6 shows the relative entropy calculated at each point between the

299   evaporative source averaged over just the three driest years, based on GPCP

300   precipitation, and the 27-year climatological evaporative source. The calculation is

301   performed on the lower-resolution GPCP data grid, and only differences significant

302   at the 90% confidence level are shown. Significance is estimated by a Monte Carlo

303   method, where the mean evaporative source and that for each of the 27 individual

304   years, for each season, are used to calculate relative entropies, and the mean and

305   standard deviation of the 27 values are calculated at each point. This is then

306   compared to the same calculations made for each combination of 3 years, a sample

307   size of 2,925, but only for a subsample of 100 points and seasons (computational

308   expense is otherwise prohibitive). Assuming the variability of relative entropy is

309   normally distributed, and that a linear transform can be used for the means and

310   standard deviations between the combinations of 27 taken three at a time and

311   combinations of 27 taken one at a time, we scale the significance thresholds.

312   The largest values of relative entropy are over arid and semi-arid regions,

313   suggesting when these areas suffer drought, there are large changes in the pattern

314   of evaporative moisture sources.   Humid areas show smaller values, and thus

315   smaller absolute variations in the patterns of evaporative moisture sources.

316   However, the areas of significant variations are widespread and not limited to any

317   specific climate regime.   Nevertheless, some general patterns emerge.   During DJF,

318   there is little significant connection between changing moisture sources and

319   drought across the Southern Hemisphere.   Summer is also the season with the least

320   coverage of significant moisture transport across most of the Northern Hemisphere.

321   At high latitudes in winter, changing moisture sources are significant.   This is

322   consistent with the strong limitations on precipitable water in the Clausius

323   Clapeyron relationship; in cold regions and seasons, precipitation is strongly

324   correlated with temperature, which is often tied to prevalent wind direction.   We

325   also see that monsoon regions in North America and Asia, and to a lesser extent

326   Africa, show significant relative entropies in the transition seasons, where late

327   onsets or early retreats of monsoon rains seem to be connected to circulation

328   anomalies.

329   The same relative entropy calculations were performed for the three wettest years

330   at each location, shown in Fig 7.   Here we find few points with statistically

331   significant changes in evaporative sources. The reason for this is straightforward.

332   Whereas droughts are the result of a deficit of precipitation over an extended period

333   of time, typically several months or more, floods often result from one or a few very

334   heavy precipitation events occurring over brief periods of days. A wet month or

335   season could be the result of an anomalous moisture source, like that brought by

336   "atmospheric rivers", which lasts only a few days. These events can easily become

337   lost when monthly or seasonal statistics are calculated.

338   Seasonal mean values of relative entropy were recalculated using the original

339   pentad-by-pentad estimates of evaporative sources over a portion of North America.

340   The results for the three wettest cases, based on pentad GPCP precipitation data, are

341   shown in Fig 8. No significance test has been applied. In all seasons, changes in the

342   evaporative source are a larger factor in flood events over the mountainous areas of

343   the West and over much of Canada than the rest of the United States. Spring is the

344   peak season for circulation changes to be associated with floods over the eastern

345   U.S. Over the North American monsoon region, relative entropy peaks during spring

346   and reaches a minimum in fall.

347   The impact of the choice of time scale is clearly evident in Fig 9. The figure shows

348   the natural logarithm of the ratio of the relative entropy at each point – pentad

349   versus monthly.   Positive values dominate, indicating that changes in the

350   evaporative source regions are more of a factor in precipitation anomalies on

351   pentad intervals than monthly. Overall, the discrepancy is greatest during JJA,

352   especially over the monsoon region and the southeastern United States. During SON

353   there is a peak along the coastlines of the southern Gulf of Mexico, coincident with

354   the season of frequent tropical storm landfall in that region. The minimum impact is

355   during DJF for most regions, although over the Northwest the discrepancies are

356   large in all seasons.

357

5. Discussion

358

359   The quasi-isentropic back trajectory scheme of Brubaker et al. (2001) has been

360   applied to data from MERRA. Estimates of the surface evaporative sources of

361   moisture supplying precipitation over land for the period 1979-2005 are presented.

362   Results are consistent with previous analyses (e.g., Brubaker et al. 2001; Dirmeyer

363   and Brubaker 2007, Dirmeyer and Kinter 2010), but the higher spatial resolution of

364   the MERRA data set reveals more structure. Systematic biases in MERRA

365   precipitation have a large effect on the surface water budget, which also impact the

366   estimates of evaporative sources. Thus, precipitation estimates have been corrected

367   using gridded data from GPCP, and evaporation data come from the MERRA-Land

368   offline replay also driven by observationally-based precipitation.

369   The methodology allows for estimates of moisture recycling and the partitioning of

370   local precipitation between terrestrial and oceanic sources, as well as estimates of

371   the distance over which moisture typically travels in the atmosphere prior to falling

372   as precipitation over any location. Recognizing that the two-dimensional

373   distributions of evaporative moisture source are tantamount to probability

374   distributions, we have used the statistical metric of relative entropy to compare

375   evaporative sources for any region under different conditions; namely cases of

376   drought or flood based on local precipitation anomalies.

377   We find that changes in local and remote surface evaporative sources of moisture

378   supplying precipitation over land are more a factor behind droughts than wet

379   anomalies over most regions of the globe. Examining results grouped by season,

380   much of the globe shows significant differences in evaporative moisture sources for

17

381   the driest ~10% (3 out of 27) of the time periods. On the other hand, very little area

382   appears to pass significance tests for comparable wet anomalies. Some of this

383   discrepancy is due to the difference in time scales underpinning droughts and floods

384   – when pentad data are considered instead of monthly data, relative entropy

385   estimates for floods increase.

386   The finding that droughts are more strongly tied to changes in evaporative sources

387   than floods seems to run counter to previous findings with this method linking

388   floods to anomalous advection of moisture (e.g., Dirmeyer et al. 1999; Reale et al.

389   2001; Turato et al. 2004; Dirmeyer and Kinter 2009, 2010), and more generally the

390   link between "atmospheric rivers" and extreme precipitation events. It may be that

391   our screening for the wettest years conflates such cases with extreme rainfall events

392   that have more localized causes. In this study, we have not tried to identify specific

393   cases of atmospheric rivers as those previous studies did. Rather, we conditioned

394   the data based simply on a ranking of precipitation amounts.

395   To try to discern whether there is more of a change in moisture transport for

396   droughts than floods, we revisit the metric shown in Fig 4 – mean distance to the

397   evaporative source. Distances to the center of mass of evaporative sources have

398   been calculated for the three wettest and driest years for each month, the same

399   cases as in Figs 5 and 6, and then averaged for seasons. The differences in the mean

400   distances (wet minus dry), expressed as a percentage of the 27-year climatological

401   mean distance to evaporative source, are shown in Fig 10. On average, distances to

402   moisture sources are greater during droughts than wet periods – as much as 12%

403   during SON for the global mean. Distances are actually greater, averaged globally,

404   for both extremes, but the differences from climatology for wet cases are less than

405   half that for droughts on average. The figure shows that there are significant

406   regional variations. Semi-arid and arid regions, where precipitable moisture often

407   has a relatively long path, generally have more distant fetches during droughts than

408   wet intervals (blue shading). This may reflect the near-total lack of evaporation in

409   the drought regions, meaning any moisture must come from relatively farther away.

410   When conditions are wet, there can be excess local evaporation. Indeed,

411   calculations of the difference between wet conditions and climatology (not shown)

412   indicate moisture transport distances are shorter over arid zones.

413   Previous studies have suggested that floods over the eastern United States may tap

414   more distant sources of moisture from the Caribbean Sea (e.g., Brubaker et al. 2001;

415   Dirmeyer and Kinter 2010), and Fig 10 supports that conclusion. Yet we do not see

416   a similar signal for California and the West coast in winter, where long "atmospheric

417   rivers" are often implicated in floods. Other red shaded regions also tap more

418   distant moisture sources during wet periods than dry.

419   Significant changes in evaporative moisture sources found in this analysis during

420   times of drought could have several causes. The calculation of evaporative sources

421   depends not only on the atmospheric circulation (horizontal wind field), but also on

422   column integrated precipitable water and surface evaporation rates, which are used

423   to determine the contribution of each upstream grid box to the overall moisture

424   supply for downstream precipitation. In this study, we have not attempted to

425   differentiate between these dynamical and hydrological factors, and even in Fig 10

426   they remain conflated.

427 Furthermore, a lack of significant contribution to precipitation extremes from

428 changing moisture transport, estimated using relative entropy, does not indicate

429 what other phenomena may be the cause. Alternative factors may include local

430 increases in atmospheric stability (buoyancy or shear), regional changes such as

431 large-scale subsidence, increased entrainment of dry air at the top of an otherwise

432 favorable boundary layer, or a change in coupled land-atmosphere feedbacks caused

433 by anomalous land surface conditions. Further diagnoses would be helpful to better

434 understand the combination of events that contribute to precipitation extremes

435 around the globe.

438

439 **References:**

440 Bagley, J. E., A. R. Desai, P. A. Dirmeyer, and J. A. Foley, 2012: Effects of land cover

441   change on precipitation and crop yield in the world's breadbaskets. Env. Res.

442   Lett., 7, 014009, doi: 10.1088/1748-9326/7/1/014009.

443 Bisselink, B., and A. J. Dolman, 2008: Precipitation recycling: Moisture sources over

444   Europe using ERA-40 data. J. Hydrometeor., 9, 1073-1083.

445 Bosilovich, M. G., and W.-Y. Sun, 1999: Numerical simulation of the 1993

446   midwestern flood: Local and remote sources of water. J. Geophys. Res., 104,

447   19415-19423.

448 Bosilovich, M. G., and S. D. Schubert, 2002: Water vapor tracers as diagnostics of the

449   regional hydrologic model. J. Hydrometeor., 3, 149-165.

450 Brubaker, K. L., D. Entekhabi, and P. S. Eagleson, 1993: Estimation of continental

451   precipitation recycling. *J. Climate*, **6**, 1077-1089.

452 Brubaker, K. L., P. A. Dirmeyer, A. Sudradjat, B. Levy, and F. Bernal, 2001: A 36-year

453   climatology of the evaporative sources of warm-season precipitation in the

454   Mississippi River Basin. J. Hydrometeor., 2, 537-557.

455 Budyko, M. I., , 1974: . Climate and Life, Academic Press, New York, 508 pp.

456 Burde, G. I., A. Zangvil, and P. J. Lamb, 1996: Estimating the role of local evaporation

457   in precipitation for a two-dimensional region. J. Climate, 9, 1328-1338.

458 Burde, G. I., and A. Zangvil, 2001: The estimation of regional precipitation recycling.

459   Part II: A new recycling model. J. Climate, 14, 2509-2527.

460   Decker, M., M. Brunke, Z. Wang, K. Sakaguchi, X. Zeng, and M.G. Bosilovich, 2012:

461   Evaluation of the reanalysis products from NCEP, ECMWF, and NASA using flux

462   tower observations. J. Climate, 25, 1916-1944, doi:10.1175/JCLI-D-11-00004.1.

463   DelSole, T., and M. K. Tippett, 2007: Predictability: Recent insights from information

464   theory. Rev. Geophys., 45, RG4002.

465   Dettinger, M. D., F. M. Ralph, T. Das, P. J. Neiman, and D. Cayan, 2011: Atmospheric

466   rivers, floods, and the water resources of California. Water, 3, 455-478.

467   Dirmeyer, P. A., and K. L. Brubaker, 1999: Contrasting evaporative moisture sources

468   during the drought of 1988 and the flood of 1993. J. Geophys. Res., 104, 19383-

469   19397.

470   Dirmeyer, P. A., and K. L. Brubaker, 2007: Global characterization of the hydrologic

471   cycle from a quasi-isentropic back-trajectory analysis of atmospheric water

472   vapor. J. Hydrometeor. 8, 20-37.

473   Dirmeyer, P. A., K. L. Brubaker, and T. DelSole, 2009: Import and export of

474   atmospheric water vapor between nations. J. Hydrol., 365, 11-22.

475   Dirmeyer, P. A., and J. L. Kinter III, 2009: The Maya Express - Late spring floods in

476   the US Midwest. Eos – Transactions of the American Geophysical Union, 90, 101-

477   102.

478   Dirmeyer, P. A., and J. L. Kinter III, 2010: Floods over the US Midwest: A regional

479   water cycle perspective. J. Hydrometeor., 11, 1172-1181.

480   Dirmeyer, P. A., 2011: The terrestrial segment of soil moisture-climate coupling.

481   Geophys. Res. Lett., 38, L16702, doi: 10.1029/2011GL048268.

482   Dominguez, F., P. Kumar, X.-Z. Liang, and M. Ting, 2006: Impact of atmospheric

483   moisture storage on precipitation. J. Climate, 19, 1513-1530.

484   Druyan, L. M., and R. D. Koster, 1989: Sources of Sahel precipitation for simulated

485   drought and rainy seasons. J. Climate, 2, 1438-1446.

486   Ducharne, A., R. D. Koster, M. J. Suarez, M. Stieglitz, and P. Kumar, 2000: A

487   catchment-based approach to modeling land surface processes in a general

488   circulation model, 2, Parameter extimation and model demonstration. J. Geophys.

489   Res., 105, 24823-24838.

490   Eltahir, E. A. B., and R. L. Bras, 1994: Precipitation recycling in the Amazon Basin.

491   Quart. J. Roy. Meteor. Soc., 120, 861-880.

492   Gimeno, L., A. Drumond, R. Nieto, R. M. Trigo, and A. Stohl, 2010: On the origin of

493   continental precipitation. Geophys. Res. Lett., 37, L13804, doi:

494   10.1029/2010GL043712.

495   Gimeno, L., A. Stohl, R. M. Trigo, F. Dominguez, K. Yoshimura, L. Yu, A. Drumond, A.

496   M. Durán-Quesada, and R. Nieto, 2012: Oceanic and terrestrial sources of

497   continental precipitation. Rev. Geophys., 50, RG4003, doi:

498   10.1029/2012RG000389.

499   Goessling, H. F. and C. H. Reick, 2011: What do moisture recycling estimates tell us?

500   Exploring the extreme case of non-evaporating continents. Hydrol. Earth Syst.

501   Sci., 15, 3217-3235, doi: 10.5194/hess-15-3217-2011.

502   Gong, C., and E. Eltahir, 1996: Sources of moisture for rainfall in West Africa. Water

503   Resour. Res., 32, 3115-3121.

504   Henderson-Sellers, A., K. McGuffie, D. Noone, and P. Irannejad, 2004: Using stable

505   water isotopes to evaluate basin-scale simulations of surface water budgets. J.

506   Hydrometeor., 5, 805-822.

507   Huffman, G. J., R. F. Adler, D. T. Bolvin, and G. Gu, 2009: Improving the global

508   precipitation record: GPCP Version 2.1, Geophys. Res. Lett., 36, L17808,

509   doi:10.1029/2009GL040000.

510   Kanamitsu, M., W. Ebisuzaki, J. Woollen, S.-K. Yang, J. J. Hnilo, M. Fiorino, and G. L.

511   Potter, 2002: NCEP-DOE AMIP-II reanalysis (R-2). Bull. Amer. Meteor. Soc., 83,

512   1631-1648.

513   Keys, P. W., R. J. van der Ent, L. J. Gordon, H. Hoff, R. Nikoli, and H. H. G. Savenije,

514   2012: Analyzing precipitationsheds to understand the vulnerability of rainfall

515   dependent regions. Biogeosci., 9, 733-746.

516   Kleeman, R., 2002: Measuring dynamical prediction utility using relative entropy. J.

517   Atmos. Sci., 59, 2057-2072.

518   Koster, R. D., M. J. Suarez, A. Ducharne, M. Stieglitz, and P. Kumar, 2000: A

519   catchment-based approach to modeling land surface processes in a general

520   circulation model, 1, Model structure. J. Geophys. Res., 105, 24809-24822.

521   Kurita, N., N. Yoshida, G. Inoue, and E. A. Chayanova, 2004: Modern isotope

522   climatology of Russia: A first assessment. J. Geophys. Res., 109, D03102, doi:

523   10.1029/2003JD003404.

524   Numaguti, A., 1999: Origin and recycling processes of precipitating water over the

525   Eurasian continent: Experiments using an atmospheric general circulation model.

526   J. Geophys. Res., 104, 1957-1972.

527   Reale, O., L. Feudale, and B. Turato, 2001: Evaporative moisture sources during a

528   sequence of floods in the Mediterranean region. Geophys. Res. Let., 28, 2085-

529   2088.

530   Reichle, R. H., R. D. Koster, G. J. M. De Lannoy, B. A. Forman, Q. Liu, S. P. P. Mahanama,

531   and A. Touré, 2011: Assessment and enhancement of MERRA land surface

532   hydrology estimates. J. Climate, 24, 6322–6338.

533   Rienecker, M. M., and Coauthors, 2011: MERRA: NASA's Modern-Era Retrospective

534   Analysis for Research and Applications. J. Climate, 24, 3624–3648.

535   Robertson, F. R., M. Bosilovich, J. Chen, and T. Miller, 2011: The effect of satellite

536   observing system changes on MERRA water and energy fluxes. J. Climate, 24,

537   5197-5217, doi:10.1175/2011JCLI4227.1.

538   Salati, E., A. Dall'Olio, E. Matsui, and J. Gat, 1979: Recycling of water in the Amazon

539   Basin: an isotopic study. Water Resour. Res., 15, 1250-1258.

540   Spracklen, D. V., S. R. Arnold, and C. M. Taylor, 2012: Observations of increased

541   tropical rainfall preceded by air passage over forests. Nature, 489, 282-286.

542   Stohl, A. and P. James, 2004: A Lagrangian analysis of the atmospheric branch of the

543   global water cycle. Part I: Method description, validation, and demonstration for

544   the August 2002 flooding in Central Europe. J. Hydrometeor., 5, 656-678.

545   Stohl, A. and P. James, 2005: A Lagrangian analysis of the atmospheric branch of the

546   global water cycle. Part II: Moisture transport between earth's ocean basins and

547   river catchments. J. Hydrometeor., 6, 961-984.

548   Sudradjat, A., 2002: Source-sink analysis of precipitation supply to large river

549   basins. PhD Dissertation, [Available from University of Maryland, College Park,

550   MD 20742, U.S.A.], 186 pp.

551   Sudradjat, A., K. L. Brubaker, and P. A. Dirmeyer, 2003: Interannual variability of

552   surface evaporative moisture sources of warm-season precipitation in the

553   Mississippi River Basin.. J. Geophys. Res., 108, doi: 10.1029/2002JD003061.

554   Tian, L., V. Masson-Delmotte, M. Stievenard, T. Yao, and J. Jouzel, 2001: Tibetan

555   Plateau summer monsoon northward extent revealed by measurements of water

556   stable isotopes. J. Geophys. Res., 106, 28081-28088.

557   Trenberth, K. E., 1999: Atmospheric moisture recycling: Role of advection and local

558   evaporation. J. Climate, 12, 1368-1381.

559   Tuinenburg, O. A. , R. W. A. Hutjes, and P. Kabat, 2012: The fate of evaporated water

560   from the Ganges basin. J. Geophys. Res., 117, D01107, doi:

561   10.1029/2011JD016221.

562   Turato, B., O. Reale, and F. Siccardi, 2004: Water vapor sources of the October 2000

563   Piedmont flood. J. Hydrometeor., 5, 693-712.

564   van der Ent, R. J., H. H. G. Savenije, B. Schaefli, and S. C. Steele-Dunne, 2010: Origin

565   and fate of atmospheric moisture over continents. Water Resour. Res., 46,

566   W09525, doi: 10.1029/2010WR009127.

567   Wei, J., P. A. Dirmeyer, M. J. Bosilovich, and R. Wu. 2012: Water vapor sources for

568   Yangtze River Valley rainfall: Climatology, variability, and implications for rainfall

569   forecasting, J. Geophys. Res., 117, D05126, doi:10.1029/2011JD016902.

570   Wei, J., P. A. Dirmeyer, D. Wisser, M. J. Bosilovich, and D. M. Mocko, 2013: Where

571   does the irrigation water go? An estimate of the contribution of irrigation to

572   precipitation using MERRA. J. Hydrometeor., 14, 275-289, doi: 10.1175/JHM-D-

573   12-079.1.

574   Xie, P., J. E. Janowiak, P. A. Arkin, R. Adler, A. Gruber, R. Ferraro, G. J. Huffman, and S.

575   Curtis , 2003: Gauge-based monthly analysis of global land precipitation from

576   1971 to 1994. J. Climate, 16, 2197-2214.

577   Yoshimura, K., T. Oki, N. Ohte, and S. Kanae, 2004: Colored moisture analysis

578   estimates of variations in 1998 Asian monsoon water sources. J. Meteor. Soc.

579   Japan, 82, 1315–1329.

580

Figure Captions:

582 Figure 1. Top panels: total seasonal evaporative source (kg m^{-2}) for all precipitation

583   over ice-free land based on MERRA atmospheric data with MERRA-Land

584   evaporation and precipitation estimates. Bottom panels: Difference when all data

585   from MERRA are used instead.

586 Figure 2: 27-year mean evaporative source for precipitation over the outlined

587   states, expressed as the fraction of total originating from each MERRA grid box

588   (normalized so the global sum for each equals 1). The two contours represent 50

589   and 100 parts per million, shading indicates greater than 200 and 300 parts per

590   million.

591 Figure 3: Fraction of precipitation originating as evaporation over land.

592 Figure 4: Distance to the center of mass of the mean evaporative source distribution

593   for each land grid point (km) for DJF (top) and JJA (bottom).

594 Figure 5: The average relative entropy at each point calculated between the

595   climatological evaporative moisture source and the source for each of the 27

596   years. Large values indicate greater interannual variability in the source of

597   moisture supplying local precipitation.

598 Figure 6. Relative entropy between the climatological evaporative source

599   distribution and the evaporative source distribution for the three driest years,

600   calculated for each ice-free land grid point using monthly data and then averaged

601   for each season. Regions with climatological rainfall rates less than 0.1 mm/day

602   are masked. Areas where the relative entropy is not significant at the 90%

603   confidence level are shaded dark grey.

604   Figure 7. As in Fig 6, for the wettest three years.

605   Figure 8. As in Fig 7, but calculated using pentad instead of monthly data. No

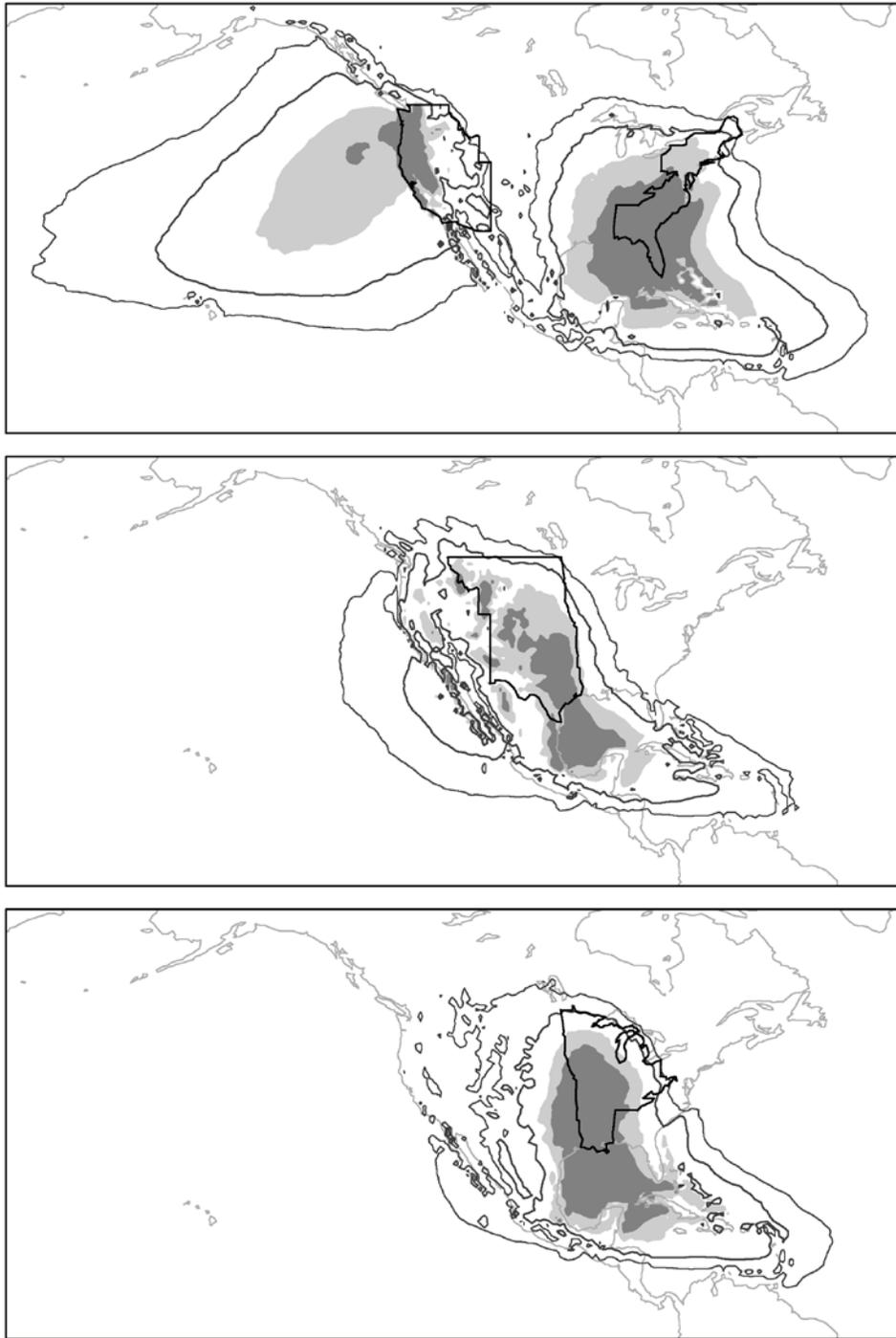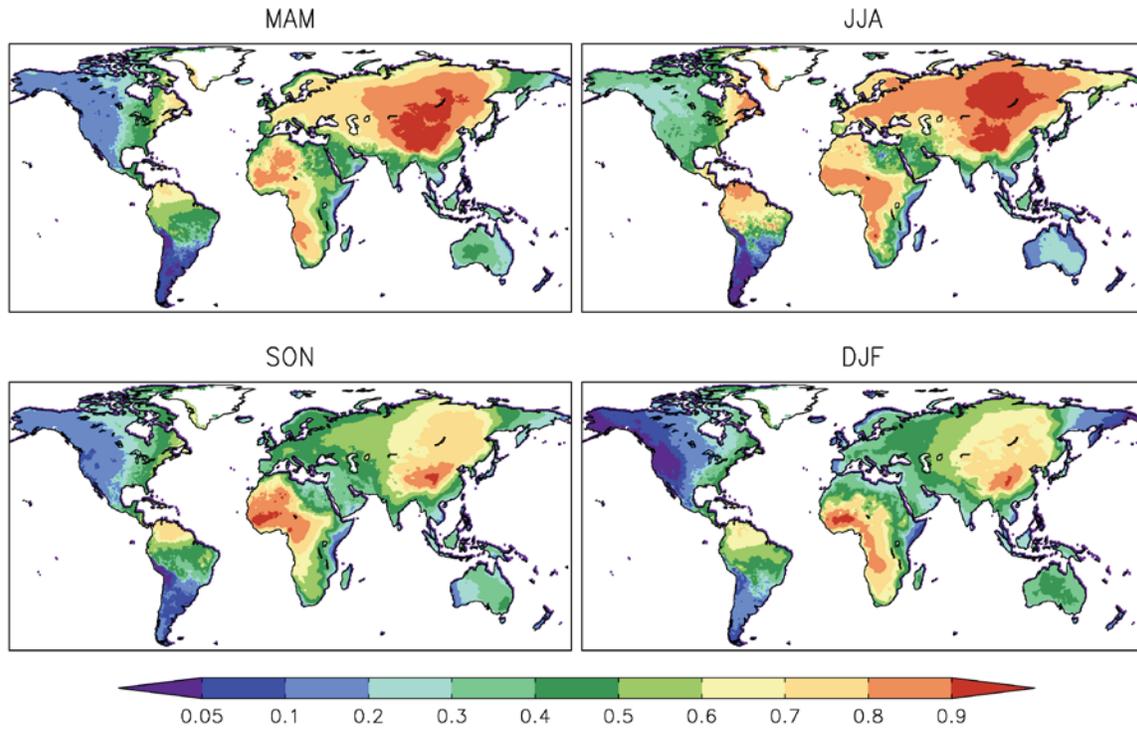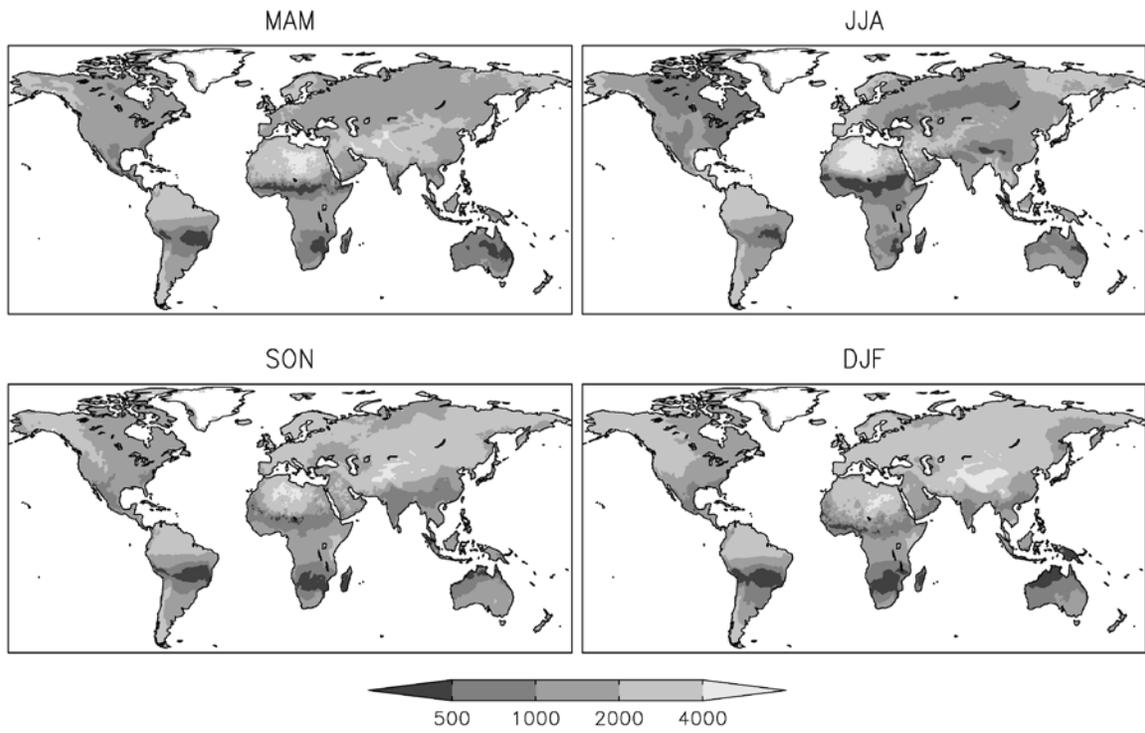606   significance screening has been applied.

607   Figure 9. The natural logarithm of the ratio of the relative entropy calculated with

608   pentad data over that calculated with monthly data.

609   Figure 10: Difference (three wettest minus three driest years) in the average

610   distance between precipitation at each land point and the evaporative source

611   supplying that precipitation, expressed as a percentage of the climatological

612   average distance. Positive values indicate dry conditions have closer moisture

613   sources than wet.

614
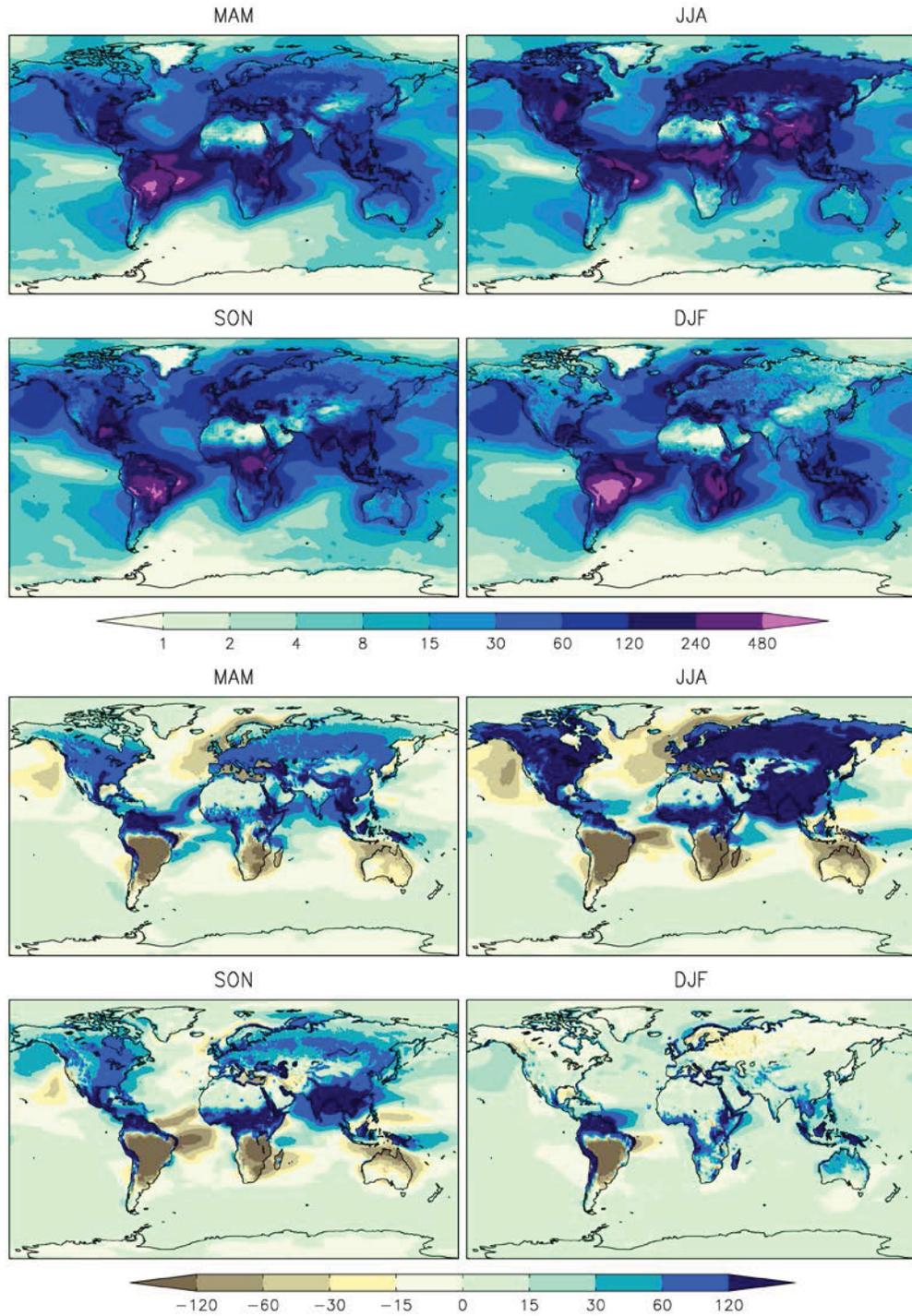
615 Figure 1. Top panels: total seasonal evaporative source (kg m^{-2}) for all precipitation
616   over ice-free land based on MERRA atmospheric data with MERRA-Land
617   evaporation and precipitation estimates. Bottom panels: Difference when all data
618   from MERRA are used instead.

619

Figure 2: 27-year mean evaporative source for precipitation over the outlined states, expressed as the fraction of total originating from each MERRA grid box (normalized so the global sum for each equals 1). The two contours represent 50 and 100 parts per million, shading indicates greater than 200 and 300 parts per million.

627
628   Figure 3: Fraction of precipitation originating as evaporation over land.
629

Figure 4: Distance to the center of mass of the mean evaporative source distribution
for each land grid point (km).

Figure 5: The average relative entropy at each point calculated between the climatological evaporative moisture source and the source for each of the 27 years. Large values indicate greater interannual variability in the source of moisture supplying local precipitation.

Figure 6. Relative entropy between the climatological evaporative source distribution and the evaporative source distribution for the three driest years, calculated for each ice-free land grid point using monthly data and then averaged for each season. Regions with climatological rainfall rates less than 0.1 mm/day are masked. Areas where the relative entropy is not significant at the 90% confidence level are shaded dark grey.
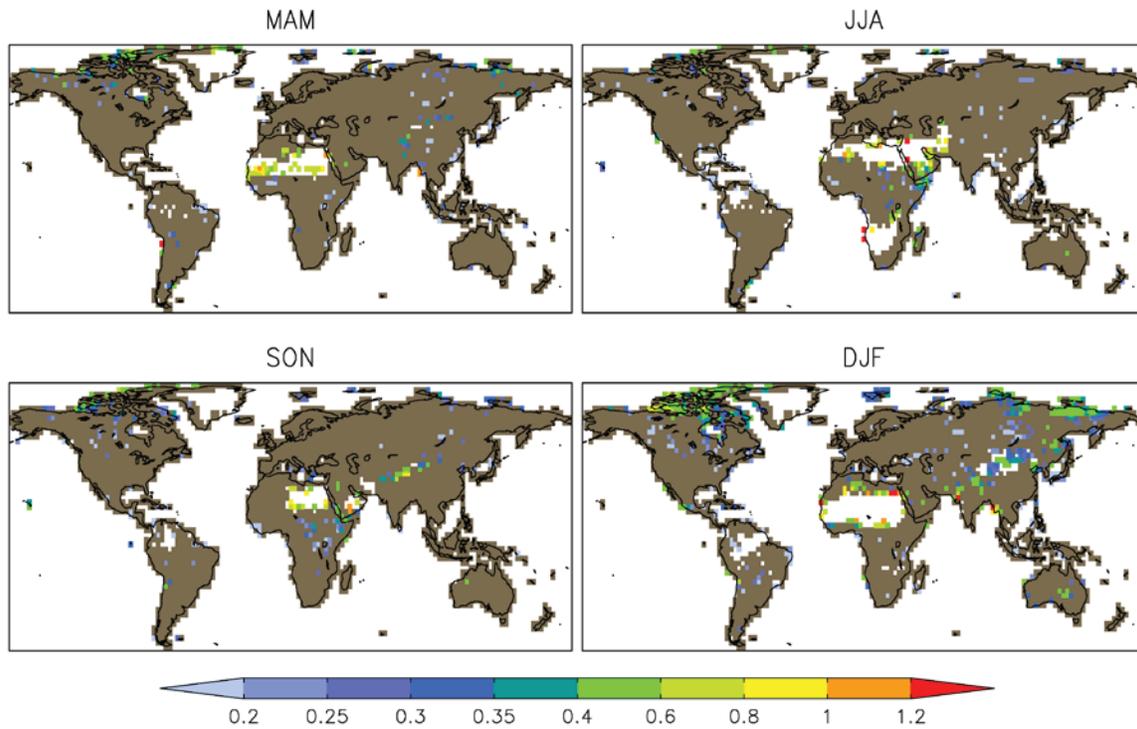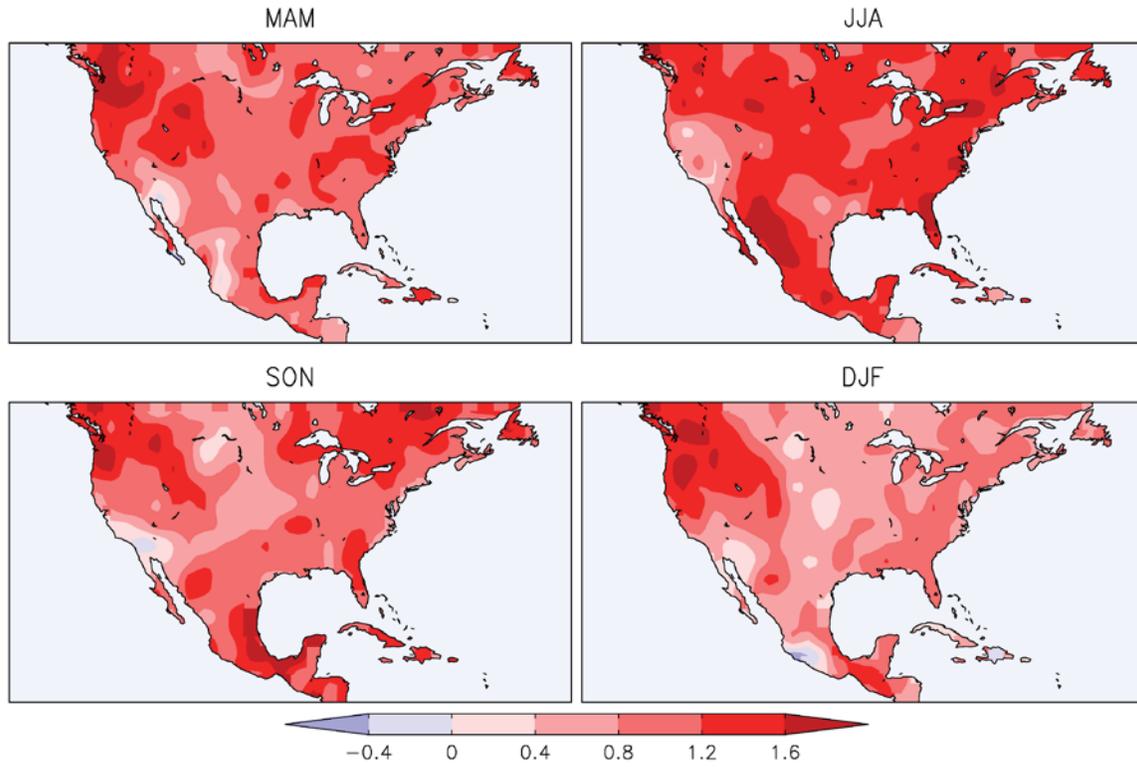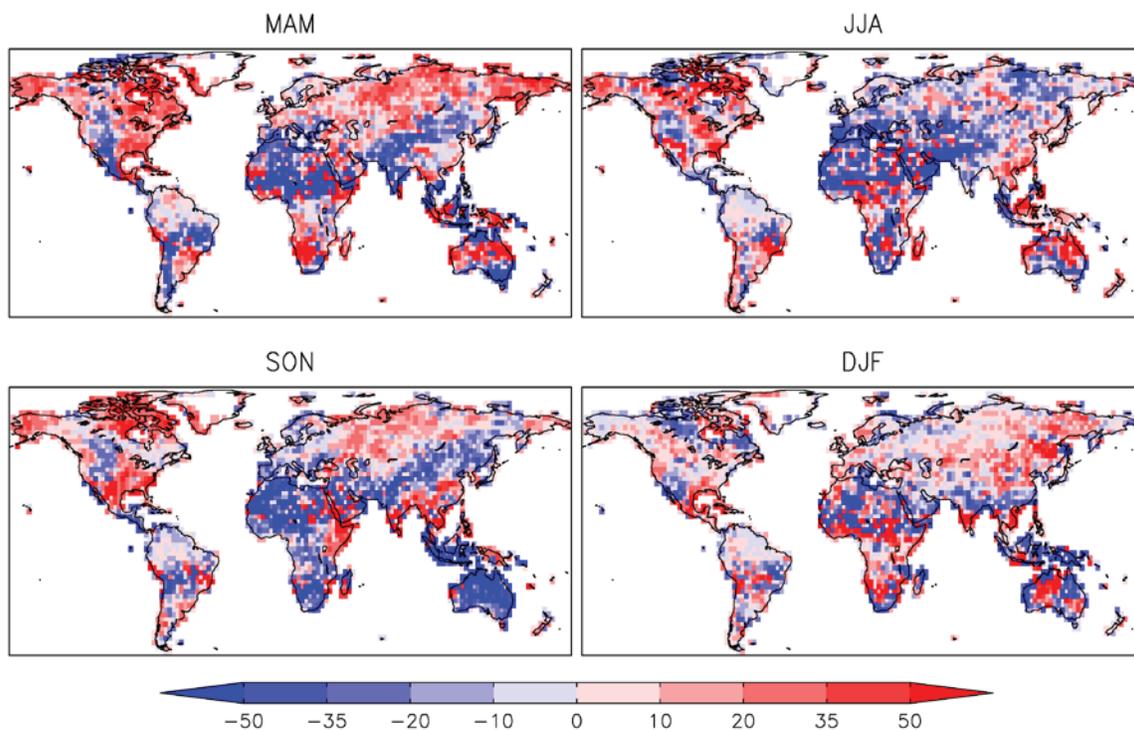
Figure 7. As in Fig 6, for the wettest three years.
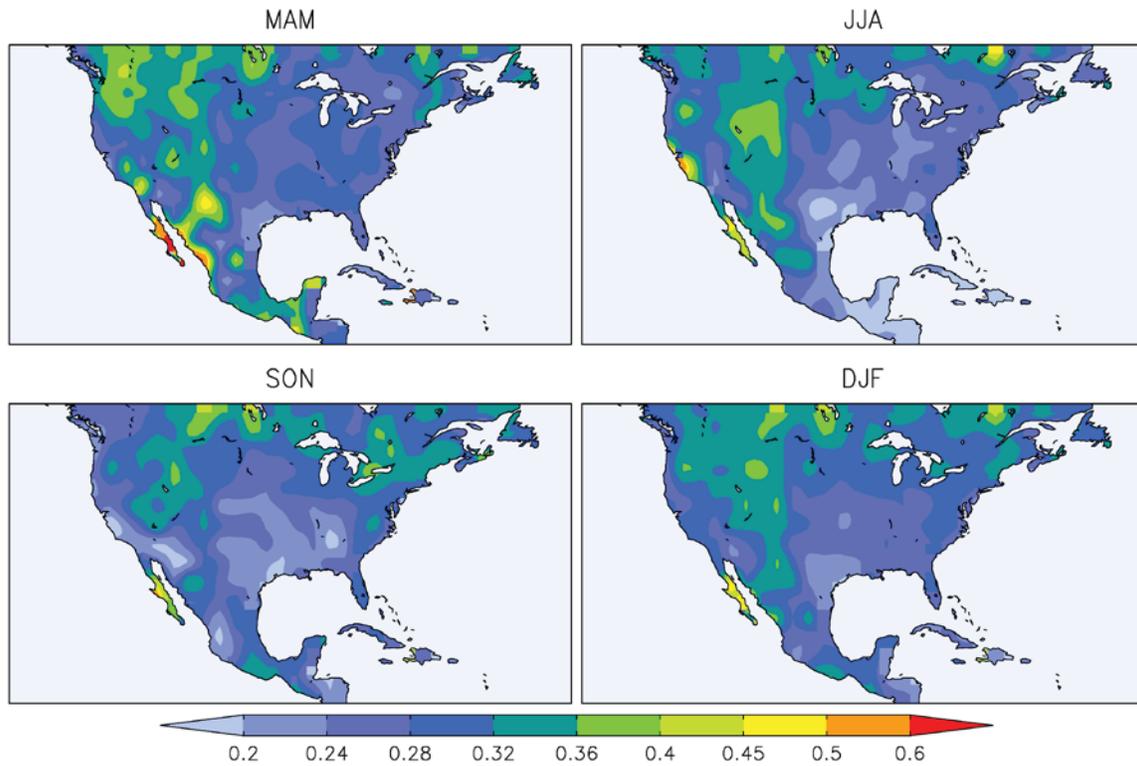
Figure 8. As in Fig 7, but calculated using pentad instead of monthly data. No significance screening has been applied.

Figure 9. The natural logarithm of the ratio of the relative entropy calculated with pentad data over that calculated with monthly data.

Figure 10: Difference (three wettest minus three driest years) in the average distance between precipitation at each land point and the evaporative source supplying that precipitation, expressed as a percentage of the climatological average distance. Positive values indicate dry conditions have closer moisture sources than wet.